Unmanned Systems, Vol. 5, No. 2 (2017) 115–127

DOI: 10.1142/S230138501750008X

UNMANNED SYSTEMS
http://www.worldscientific.com/worldscinet/us

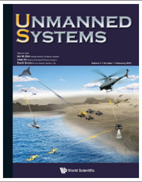

Wingbeat Generation for a 15 DOF Flexible-Wing Aerial Vehicle Using Cosine Wave Functions

Willson Amalraj Arokiasami*, Prahlad Vadakkepat†, Abdullah Al Mamun‡

Department of Electrical and Computer Engineering,
National University of Singapore, Singapore

Birds and conventional airplanes control their flight in a different manner. Conventional airplanes maneuver themselves by means of moving surfaces, while birds can bend, twist and deform their wings and adapt to unforeseen conditions such as wind gusts. However, if planes can do exactly as the birds do they can gain agility, more lift, less drag while consuming less fuel. This work aims to address this issue. Therefore, approaches of wingbeat generation for a 15 DOF flexible-wing aerial vehicle are developed in this paper. A computationally cost-effective cosine wave function-based algorithm that computes a set of wingbeats enabling the aerial vehicle to follow a desired trajectory in a realistic manner is discussed. The flexible-wing aerial vehicle is modeled similar to a seagull with an articulated skeleton. Motion of the aerial vehicle is simulated by applying joint torques and aerodynamic forces over a period of time in forward dynamics simulation. Wing and tail feather motions generate lift in the aerial vehicle, which makes it possible for the aerial vehicle to trace predefined paths. The solidworks mechanical design is used as input into Matlab SimMechanics for visualization. The results are promising for the construction of bird-like aerial vehicles.

Keywords: Bio-mimetic; flexible-wing; aerial vehicle; path tracking; cosine wave functions.

1. Introduction

A number of models are available in the literature depicting the natural motion of living creatures such as the motion of snakes [1], aquatic animals [2], dogs [3], insects [4–6], birds [7, 8] and even extinct and imaginary animals [9]. There are principles of locomotion common in birds, insects, fishes and swimmers [10, 11], but it is the lift motion (take off and landing) of birds that delineates them from insects, fishes and swimmers. Modeling the aerial motion of a flexible-wing aerial vehicle presents a significant challenge for real-time simulation as well as the design of efficient control systems [12]. The aerodynamic forces that are generated due to the interactions between birds wings and wind are complex to analyze, and slight changes in wing positions can lead to aerodynamic turbulence, thus making it difficult to study. The skeletal structure of the bird and the elastic properties of its feathers dictate its gait patterns and flight motions [13].

Wings help birds to fly. A bird's wing is curved on top and flat or slightly curved at the bottom [14]. Birds launch themselves into the air by using their leg muscles to push against a perch or to jump from the ground, flapping their wings in the process. Birds wings not only flap up and down but also twist forward while flying. This twisting motion propels the bird to fly forward. The rest of the wing remains flat in relation to airflow and so provides the lift. Some birds such as cranes continue to fly mainly by flapping their wings while others such as eagle, seagull, etc. combine flapping flights with gliding or soaring.

Aircraft designs, modeled from a bird obtain roll control by wrapping or changing the portion of the wing. The three types of most common aircraft designs are (1) Fixed-wing aircraft, (2) Flapping-wing aerial vehicles and (3) Flexible-wing aerial vehicles. In fixed-wing aircraft, the lift generated is a function of the forward airspeed, the wing span and surface area of the wing. At low Reynolds number flights (low flight air speeds less than 10 m/s), conventional fixed-wing aircraft are less efficient [15]. In flapping-wing aerial vehicles,

Received 9 April 2016; Revised 24 April 2017; Accepted 24 April 2017; Published 14 June 2017. This paper was recommended for publication in its revised form by editorial board member, Biao Wang.
Email Addresses: *willson@nus.edu.sg, †prahlad@nus.edu.sg, ‡elealm@nus.edu.sg

the lift generation originates from the flapping motion of the wing. In flapping-wing aerial vehicles and flexible-wing aerial vehicles, wingbeats control the lift generated, making it efficient for low Reynolds numbers flight [15, 16]. For flapping-wing aerial vehicles, the entire wing is considered as one joint whereas in flexible-wing aerial vehicles, one wing is made up of many individual joints. Morphing the attributes of bird wings is a priority research topic among aircraft designers nowadays [17, 18]. The research on flexible-wing aerial vehicle has been active for a long time and it gained increased attention when the Defence Advanced Research Projects Agency (DARPA) launched a program to create an aerial vehicle that could operate with a high degree of autonomy in a squad-level combat environment.

Reynolds [19] is the first one to simulate the flight of a flock of birds in a realistic manner by adopting a rule-based simulation, where the simulation of wingbeat motion is not physical. The flapping of the wings generates the required aerodynamic forces. Ramakrishnananda and Wong [20] proposed a large flapping model capable of forward motion with natural wingbeat motions. The calculation is computationally intensive and the model is capable of only forward motion. Wu and Popovic [21] then reported a realistic animation of a bird's flight, where modeling of individual feathers are also considered. The wingbeat parameters are optimized off-line using evolutionary algorithms. This optimization process require a computation time of 3–5 h per simulation in order to produce solutions for flight trajectories lasting around 10 s. Cao *et al.* [22] proposed a flapping-driven model that could trace even arbitrary paths using its tail feathers. However, a demonstration of taking off and level flight by flexible-wing systems with large number of degrees of freedom has not been reported.

To address these gaps in the research field, a flexible-wing aerial vehicle with 15 DOF skeletal structure that is biologically inspired from a fully grown seagull is considered in this work. The wingbeat and tail feather motions are simulated and results from SimMechanics show that the model is capable of performing aerial maneuvres similar to that of a bird in a realistic manner. This paper is organized as follows: Biological inspiration of the structure adopted is discussed in Sec. 2 and in subsequent sections, distinct aspects of the control algorithms are elaborated.

2. Biological Inspiration and Modeling of the Aerial Vehicle

A seven segment joint system is used to model a bird. Each wing has three segments and the trunk forms the remaining segment. Almost all the species of birds have such a wing geometry [25]. Figure 1 is a representation of the different segments and joints.

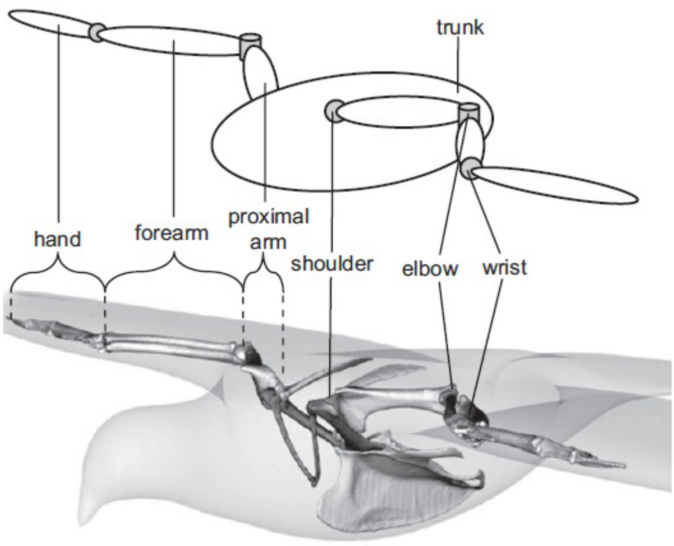

Fig. 1. Anatomical structure of a bird [23, 24].

The aerial vehicle is modeled as a formation of 9 articulated links, 4 on each of its wings and one in its tail, similar to that of a bird. The wing structure is modeled similar to the skeletal structure of a bird. The model has a quaternion joint in its shoulder and a revolute joint at the elbow, forearm and wrist, respectively, thus making up 6 DOF in each of the wings and 3 revolute joints in the tail (Table 1). The entire structure includes 15 DOFs. The location of the joints are explained in Figs. 1 and 2.

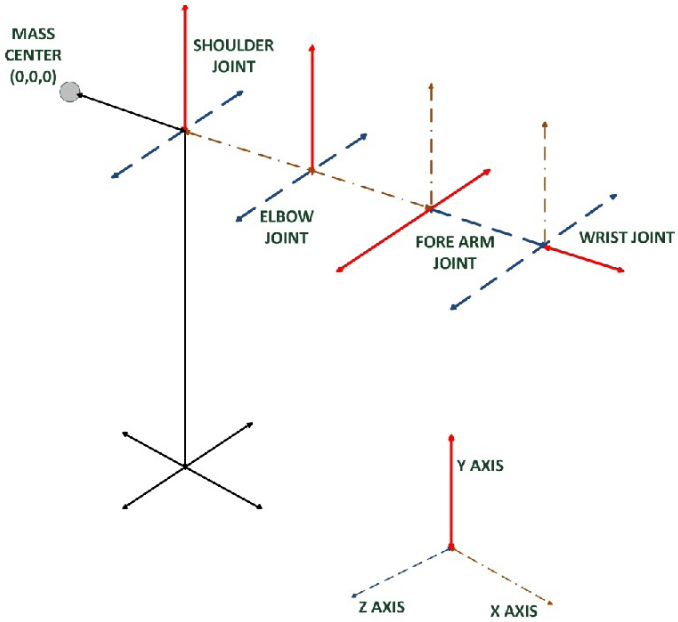

Fig. 2. Joint positions in right wing of a bird indicated in co-ordinate frames.

Table 1. Joints modeled in the structure and the number of degrees of freedom contributed by them.

	DOF	No. of joints	DOF contributed
Shoulder	3	2	6
Elbow	1	2	2
Forearm	1	2	2
Wrist	1	2	2
Tail Bend	1	1	1
Tail Twist	1	1	1
Tail Spread	1	1	1
		Total	15

In general, birds follow two gait patterns namely the Vortex-Ring gait and Continuous Vortex gait [13]. In order to realize these gait patterns, certain parameters namely the wingbeat parameters are assigned for the wing; as the control parameters need to differentiate the up stroke and down stroke motions. There are 15 such parameters, of which six parameters represent the right wing, while another six parameters represent the left wing and the remaining three parameters represent the tail. For simplicity, the joints are numbered. 1–6 represent the right wing while 7–12 represent the left wing, respectively, and 13–15 represent the tail (Table 2).

In Table 3, $u_i^{\uparrow/\downarrow}$ represent the wingbeat parameters where $u_i^{\uparrow}$ is for up-stroke and $u_i^{\downarrow}$ is for down-stroke. The maximum and minimum joint limits for each joint are represented by $\overline{u_i}$ and $\underline{u_i}$ wingbeat parameters. These limits are different for different joints. Motion of the wings varies as a function of wingbeat angle Θ, which is nothing but the arm dihedral angle. Down-stroke starts when the arm dihedral angle varies from 0° towards -90° and it ends when it varies from -90° to 0°, while up-stroke starts when the arm dihedral angle varies from 0° towards 90° and ends when it varies from 90° to 0°. One down-stroke combined with one up-stroke forms a wingbeat. For simplicity these parameters are not listed separately. Arm dihedral angle and arm sweep angle are shown in Figs. 3 and 4.

Table 2. Joint numbering.

Joint number	Definition
1, 7	Arm Dihedral
2, 8	Arm Sweep
3, 9	Arm Twist
4, 10	Elbow Bend
5, 11	Fore Arm Twist
6, 12	Wrist Bend
13	Tail Bend
14	Tail Twist
15	Tail Spread

Table 3. Wingbeat parameters.

Wingbeat parameter	Definition
$u_1^{\downarrow}, u_1^{\uparrow}$	Arm Dihedral angle
$u_2^{\downarrow}, u_2^{\uparrow}$	Arm Sweep angle
$u_3^{\downarrow}, u_3^{\uparrow}$	Arm twist
$u_4^{\downarrow}, u_4^{\uparrow}$	Elbow bend
$u_5^{\downarrow}, u_5^{\uparrow}$	Fore Arm twist
$u_6^{\downarrow}, u_6^{\uparrow}$	Wrist bend
$u_{13}^{\downarrow}, u_{13}^{\uparrow}$	Tail bend
$u_{14}^{\downarrow}, u_{14}^{\uparrow}$	Tail twist
$u_{15}^{\downarrow}, u_{15}^{\uparrow}$	Tail spread

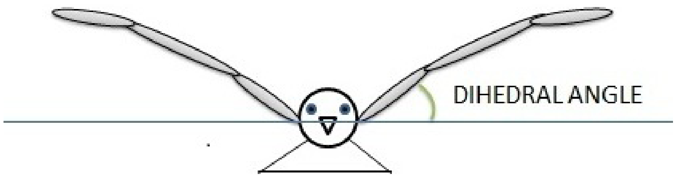

Fig. 3. Representation of arm dihedral angle.

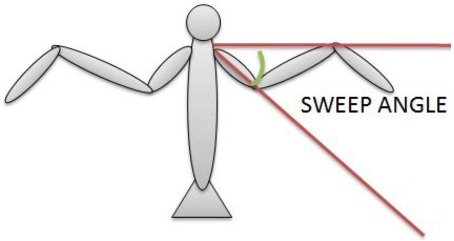

Fig. 4. Representation of arm sweep angle.

2.1. *Frequency of wingbeat*

The frequency of flapping in a bird is dependent on its anatomical structure [26]. The bird cannot follow a wingbeat frequency greater than its natural frequency as it would require more force from its muscles to overcome the drag force generated during each up-stroke. It also cannot follow a frequency lower than its natural frequency as that would make it less efficient. Pennycuick [26] devised an empirical formula that suggests the natural frequency for a particular anatomical structure of a bird.

$$f = 1.08\frac{1}{b}\left(\frac{m}{\rho}\right)^{1/3}\left(\frac{g^2}{S}\right)^{1/4}, \tag{1}$$

where f is the frequency of wingbeat, b is the wingspan, m is the mass of the bird, ρ is the air density, g is the acceleration due to gravity and S is the wing area. The maximum frequency of flapping for the aerial vehicle designed after substitution of required parameters is found to be 1.7 flapping/s. The simulation is performed at 1.5 flappings/s.

2.2. *Cosine wave function-based wingbeat parameter generation*

Reports by [27] and [28] indicate that wing tip displacement over a period in an aerial vehicle can be fit using a cosine wave curve represented by $a_{\text{TIP}}\cos(\omega+\phi)$, where a_{TIP} is the amplitude of displacement and ϕ is the negative value of the tip displacement angle. For an aerial vehicle modeled as an articulated skeleton, motion of each part of the wing can be represented using simpler cosine wave functions (Fig. 5) with varied frequency and varied amplitude. These simpler cosine wave functions are used to generate the desired wingbeat parameters for the joints. The amplitude and frequency of the cosine waves are determined based on the path to follow at the next instance as well as the co-ordinates of the mass center of the aerial-vehicle at the present instance.

The plots in Fig. 5 correspond to the wave functions pertaining to the joints in right and left wings. The X axis denotes the wingbeat angle Θ, which varies from $0°$ to $360°$ for each wingbeat and the Y axis denotes the amplitude with which each cosine wave varies. The same functions are replicated to both the wings so as to maintain symmetric wing motion. Following are the mathematical expressions of the wave functions adopted.

$$u_i^{\uparrow} = \overline{u_i}\Delta. \tag{2}$$

$$u_i^{\downarrow} = \underline{u_i}\Delta. \tag{3}$$

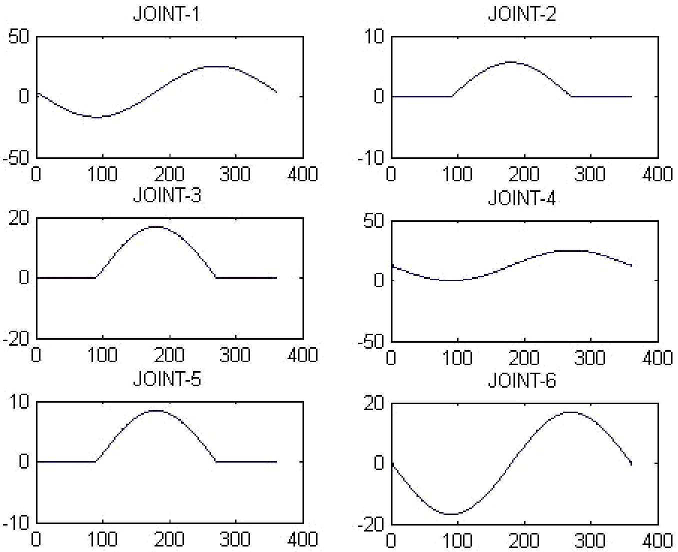

Fig. 5. Cosine wave reference functions for right and left wings.

For joints 1, 4 and 6,

$$q_{di} = (u_i^{\uparrow} - u_i^{\downarrow})\frac{1-\sin\Theta}{2} + u_i^{\downarrow}. \tag{4}$$

For joints 2, 3 and 5,

$$q_{di} = (u_i^{\uparrow} - u_i^{\downarrow})\cos\Theta + u_i^{\downarrow}, \tag{5}$$

where, $u_i^{\uparrow}$ is the wingbeat parameter during up-stroke and $u_i^{\downarrow}$ is the wingbeat parameter during down-stroke, respectively. Δ is the relative changes in amplitude expressed in percentage (for both the right and left wings). q_{di} is the desired angle for joint 'i', $\overline{u_i}$ is the maximum value of joint limitation for Joint 'i', $\underline{u_i}$ is the minimum value of joint limitation for joint 'i' and Θ is the wingbeat angle. Substituting the desired values of joint angle for all the joints at each instant in Eq. (26) as discussed in Sec. 4.2 yields the final positions of each joint, after the application of the required torque. Generation of proper desired joint angles is crucial since it has a major impact on the lift and drag forces generated during the motion of the aerial vehicle.

3. Aerodynamic Forces and the Influence of Tail Feather Motions on Aerodynamics

In this section, calculation of aerodynamic forces, their effects on aerial vehicles and the influence of tail feathers on the aerodynamics of the aerial vehicle are discussed.

3.1. *Aerodynamic forces*

Aerodynamic forces that are created during each wingbeat are determined by modeling a bird in a quasi-steady flight or unsteady flight [29]. Larger birds like the eagle, seagull, etc., usually have quasi-steady flight since their flapping frequency of the wing is low at cruising stage. Smaller birds usually have unsteady flight, since their flapping frequency, i.e., wing tip speed is greater than its flight speed [30]. Since the aerial vehicle that is under consideration in this paper has a wingspan that is comparable to that of larger birds, it is modeled with a quasi-steady flight. The aerodynamic forces like Lift force and Drag force and gravity are modeled in the system. The Angle of attack of the wing of the bird is one of the important parameter that defines the aerodynamic forces. The directions of Lift force and Drag force can be calculated as follows:

$$\bar{d} = \frac{\bar{v}}{\|\bar{v}\|}, \tag{6}$$

$$\bar{l} = \frac{\bar{d}\times\bar{n}}{\|\bar{d}\times\bar{n}\|}\times\bar{d}, \tag{7}$$

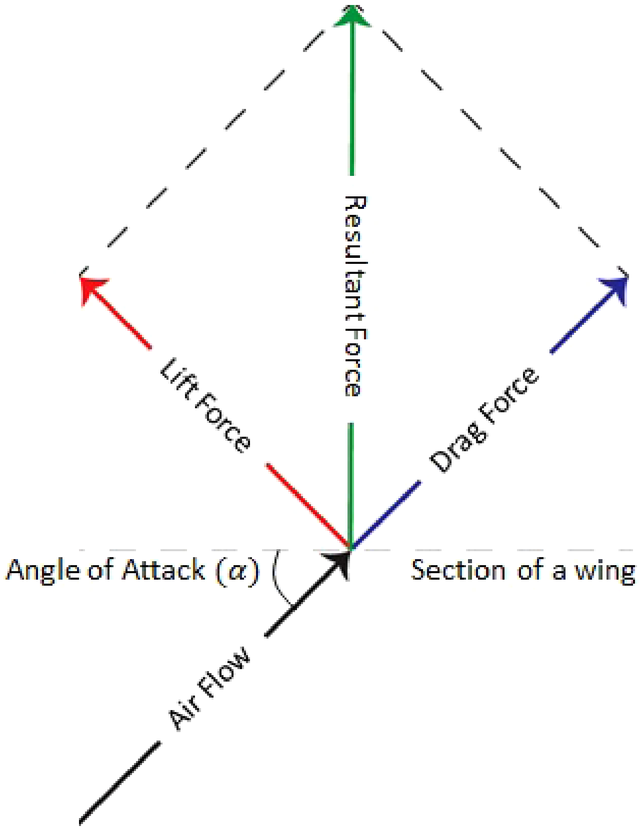

Fig. 6. Lift and Drag Forces acting on a wing surface of the wing.

where $\bar{v}$ is the direction of velocity of wind relative to the wing, $\bar{d}$ is the direction of drag force, $\bar{l}$ is the direction of lift force and $\bar{n}$ is the direction of normal to the surface at which lift and drag are calculated (Fig. 6).

Drag force acts along the direction of velocity of the wind relative to the surface and lift force acts perpendicular to the drag force. The entire wing is decomposed into four individual surfaces for simplicity. The position of all surfaces at each instant during a wingbeat is monitored and the aerodynamic forces corresponding to the angle of attack, acting on each surface are calculated. These component forces can be expressed by Eqs. (8) and (9):

$$F_L = \frac{1}{2} c_l(\alpha) \rho S \|\bar{v}\|^2 \bar{l}, \tag{8}$$

$$F_D = \frac{1}{2} c_d(\alpha) \rho S \|\bar{v}\|^2 \bar{d}, \tag{9}$$

where F_L is the lift force, F_D is the drag force, α is the angle of attack, $c_l(\alpha)$ is the lift coefficient, $c_d(\alpha)$ is the drag coefficient, ρ is the air density, S is the surface area and $\bar{v}$ is the direction of velocity of wind relative to a surface.

Lift and drag forces depend on the density of air, surface area of the segment of the wing, lift as well as drag

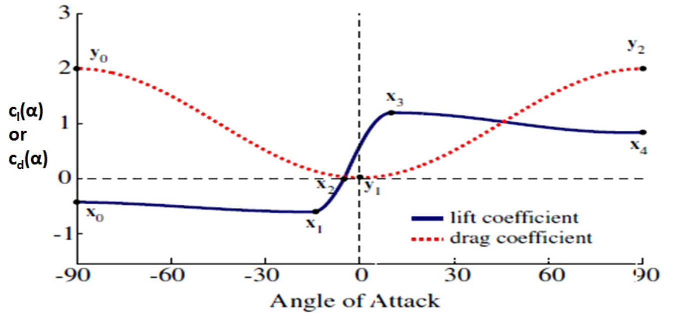

X_0	X_1	X_2	X_3	X_4	Y_0	Y_1	Y_2
(-90, -0.5)	(-10,-1.26)	(-5,0)	(15,1.8)	(-90,0.5)	(-90,2)	(0,0.02)	(90,2)

Fig. 7. Lift and Drag Coefficients plot that shows the variation lift and drag coefficients with angle of attack used in our model [21].

coefficients and velocity of wind relative to the wing. The total lift and drag forces that are acting on the entire wing surface are calculated using the blade element theory [31]. Figure 7 shows the variation of lift and drag coefficients with angle of attack used in the current model. Lift and Drag forces acting on the tail are calculated in the same manner as the forces acting on the wings (8–10). Total aerodynamic force acting on the structure is obtained by

$$F_{\text{aero}} = \sum_{i=1}^{9} F_L^i + F_D^i. \tag{10}$$

3.2. *Influence of tail on aerodynamic forces*

Tail feathers play an important role in stabilizing the flight motion of a bird. Changing the direction of flight while flying, providing compensation for lift force and increasing the drag force while landing are some of the important roles of the tail feathers. The tail contributes 3 DOF to the kinematic structure of the aerial vehicle. When the bird is turning, the tail feathers move correspondingly to the right or left in order to stabilize it. When the bird is taking off, the tail feathers close and open in sequence so as to increase lift during the upstroke and reduce drag during downstroke. The surface area of the tail feathers is changed by varying the angle of opening of tail feathers thus altering the lift and drag produced. It is important that the influence of the tail is modeled into the aerial vehicle. Figure 8 shows the various motions of tail feathers. The area of tail feathers that changes at different instances of flight motions is calculated [22] by

$$S_t = \frac{\Pi l^2 \phi}{360}, \tag{11}$$

$$\phi = 1.78 \times \max(q_{13}, q_{14}) + \bar{u}_{14}, \tag{12}$$

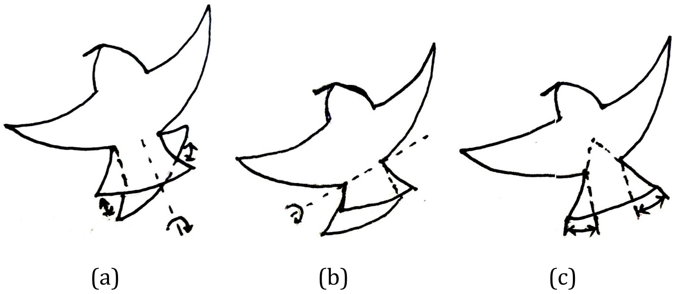

Fig. 8. Motion of tail feathers: (a) the twisting action, (b) the bending action and (c) the opening and closing of tail feathers.

where S_t is the area of tail feathers and ϕ is the opening/closing angle.

4. Equations of Motion and the Control Architecture

In this section, the equations of motions for the aerial vehicle and the control architecture used are discussed. The entire system is assumed as a rigid body system and rigid body dynamics are utilized.

4.1. *Equations of motion*

For flight dynamics and control, the reference frame is located at the center of gravity(CG), which is aligned with the aircraft and moves with it as shown in Fig. 9.

The translation along the X, Y, Z directions is denoted using the velocity vector in body axes, $V = \{u, v, w\}$ and the rotation about X, Y, Z axes is denoted using the angular velocity vector in body axes, $\omega = \{p, q, r\}$. Forces acting on the aerial vehicle are denoted by $F = \{X, Y, Z\}$. These forces act at the origin of the reference frame. Similarly the moments acting on the aerial vehicle are denoted using $M_{cg} = \{l, m, n\}$. These are the roll, pitch and yaw moments taken with respect to the CG. We can now decompose,

$$F = F_{\text{aero}} + T + W, \tag{13}$$

where F_{aero} denotes the resultant of the aerodynamic forces $X_{\text{aero}}, Y_{\text{aero}}, Z_{\text{aero}}$, T denotes the thrust T_X, T_Y, T_Z and W denotes the force due to the weight of the aerial vehicle, decomposed along the three axes as $W = Mg\{-\sin\theta \;\; \cos\theta\sin\phi \;\; \cos\theta\cos\phi\}$. Here the thrust forces acting on the aerial vehicle can be considered to be negligible compared to the other forces acting on it. The simplified linear equations of motion are given by

$$\dot{u} + qw - rv = \frac{X_{\text{aero}}}{m} - g\sin\theta, \tag{14}$$

$$\dot{v} + ru - pw = \frac{Y_{\text{aero}}}{m} - g\cos\theta\sin\phi, \tag{15}$$

$$\dot{w} + pv - qu = \frac{Z_{\text{aero}}}{m} - g\cos\theta\cos\phi. \tag{16}$$

The angular momentum of the aerial vehicle is given by

$$H_{cg} = \omega Icg, \tag{17}$$

where ω is the angular velocity of the aerial vehicle and I_{cg} is the moment of inertia of the aerial vehicle with respect to CG. Applying Coriolis theorem to $\frac{dH_{cg}}{dt} = M_{cg}$, the rotational equations of motion are,

$$\frac{\partial(\omega I_{cg})}{\partial t} + \omega \times \omega I_{cg} = M_{cg}. \tag{18}$$

Since the XY plane is symmetrical, the simplified rotational equations of motion are

$$l = I_{xx}\dot{p} + (I_{zz} - I_{yy})qr - I_{xz}(\dot{r} + pq), \tag{19}$$

$$m = I_{yy}\dot{q} + (I_{xx} - I_{zz})pr - I_{xz}(r^2 - p^2), \tag{20}$$

$$n = I_{zz}\dot{r} + (I_{yy} - I_{xx})qr - I_{xz}(\dot{p} + qr), \tag{21}$$

$$\dot{\phi} = p + (q\sin\phi + r\cos\phi)\tan\theta, \tag{22}$$

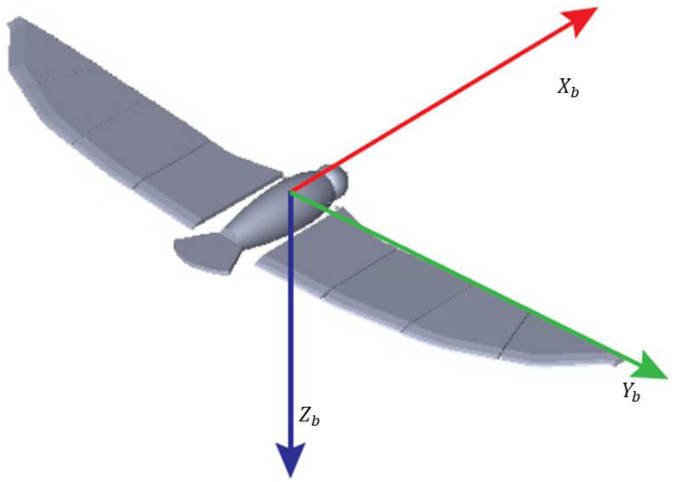

Fig. 9. Position of body frame on the aerial vehicle.

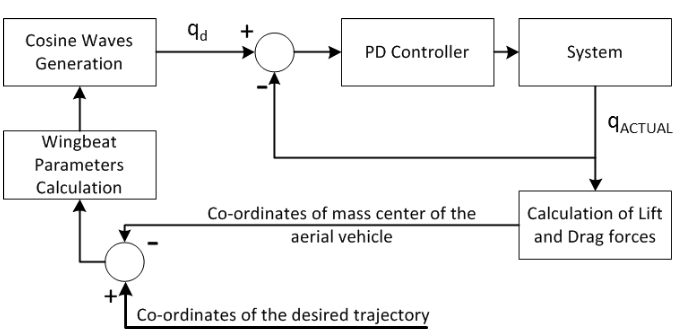

Fig. 10. Control flow diagram.

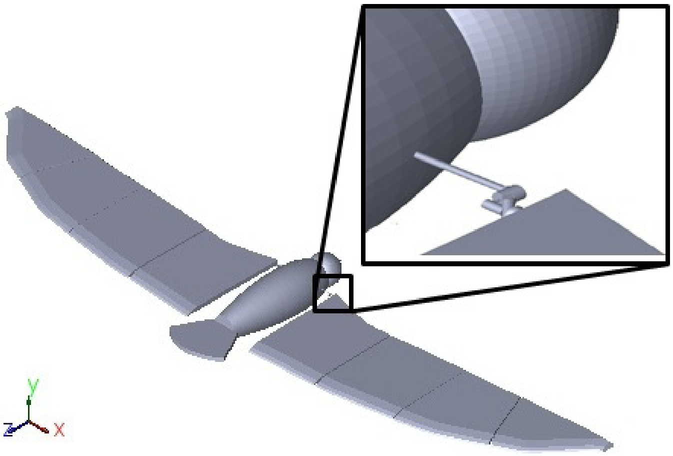

Fig. 11. Model of aerial vehicle. The inner figure shows the approximated shoulder joint.

$$\dot{\psi} = (q \sin\phi + r \cos\phi) \sec\theta, \tag{23}$$

$$\dot{\psi} = (q \sin\phi + r \cos\phi) \sec\theta. \tag{24}$$

4.2. *Architecture of the control system*

The Control system used is represented by a second order differential equation i.e.,

$$\tau = (I + \eta^2 I_m)\ddot{q} + (b + \eta^2 b_m)\dot{q}, \tag{25}$$

where $(I + \eta^2 I_m)$ is the effective inertia, $(b + \eta^2 b_m)$ is the effective damping, η is chosen as 1 (For Direct Drive) and τ is the torque. The basic idea is to use a first order cascading type PD controller of the structure,

$$q_i(t) = k_p e_i(t) + k_d \frac{d}{dt} e_i(t), \tag{26}$$

$$e_i(t) = q_{di}(t-1) - q_i(t-1), \tag{27}$$

where i is the joint number, $q_i(t)$ is the actual output, $q_{di}(t)$ is the desired output, k_p is the proportional gain and k_d is the derivative gain.

The control problem is formulated as a path tracking problem. The model is required to follow a desired trajectory. The desired trajectory is given as Cartesian co-ordinates and the mass center of the bird in Cartesian co-ordinates is monitored. It is important to note that the desired input to the PD controller is the angles which each joint has to trace and not the Cartesian co-ordinates. The conversion mechanisms which were discussed in Sec. 2.2 are employed in order to convert data from Cartesian co-ordinates into 15 angles which form the desired input q_d for the PD controller. The output of the PD controller forms the control inputs to the system. The data represented by 15 angles are converted into Cartesian co-ordinates in order to represent the mass center of the aerial vehicle at each instance.

5. Simulation Results and Discussion

In this section, two flights of aerial vehicle used in the experiment are visualized and discussed. One without a predefined trajectory and the other following a predefined trajectory.

5.1. *Visualization using SimMechanics*

The model of the aerial vehicle with dimensions approximating a seagull is developed in Solidworks and it is imported into the SimMechanics environment (Fig. 11). The quaternion joint present at the shoulders of the bird is replaced by three consecutive revolute joints of smaller dimension (Fig. 11 inset), since a quaternion joint cannot be actuated using a motor.

Fig. 12. Sequence of down-beat motions from side view.

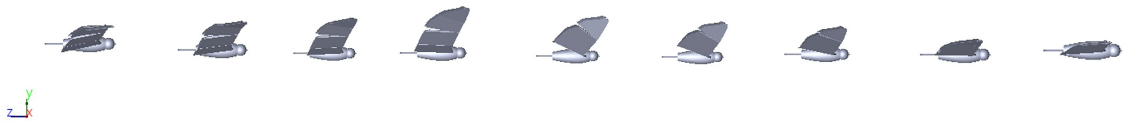

Fig. 13. Sequence of up-beat motions from side view.

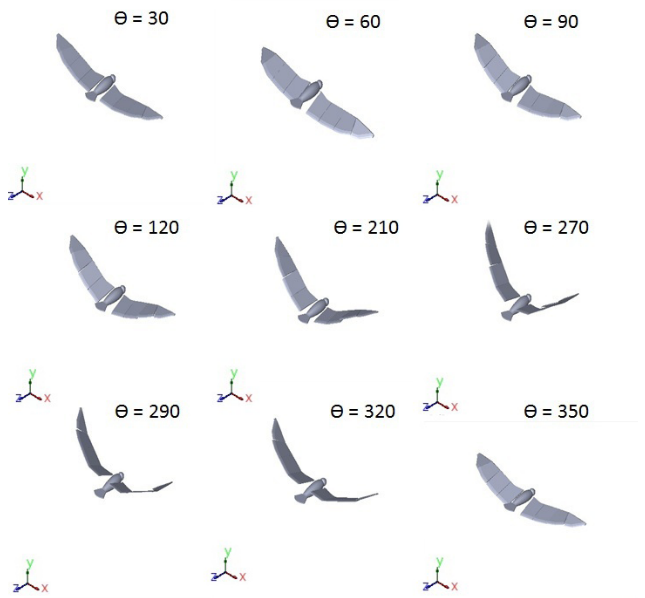

Fig. 14. Sequence of flight at various wingbeat angles — Isometric view.

In Figs. 12–14, the sequence of wingbeat motions of the aerial vehicle is shown in the side view and isometric view. These simulations are done to visualize the bird like motion of the aerial vehicle. No predefined path is considered for the aerial vehicle to follow. The aerial vehicle flaps its wings and moves forward from rest following a continuous vortex gait.

5.2. *Results on three dimensional trajectory following*

To validate the capability of the algorithm, the aerial vehicle using continuous vortex gait is made to follow three different trajectories (travel straight, turn right and turn left) individually. Wind velocity is maintained constant throughout the simulation and the disturbance to the system is considered negligible. Figures 15(a), 16(a) and 17(a) are the desired trajectories that are used in the simulation. The results that are obtained using cosine wave functions are shown in Figs. 15–17.

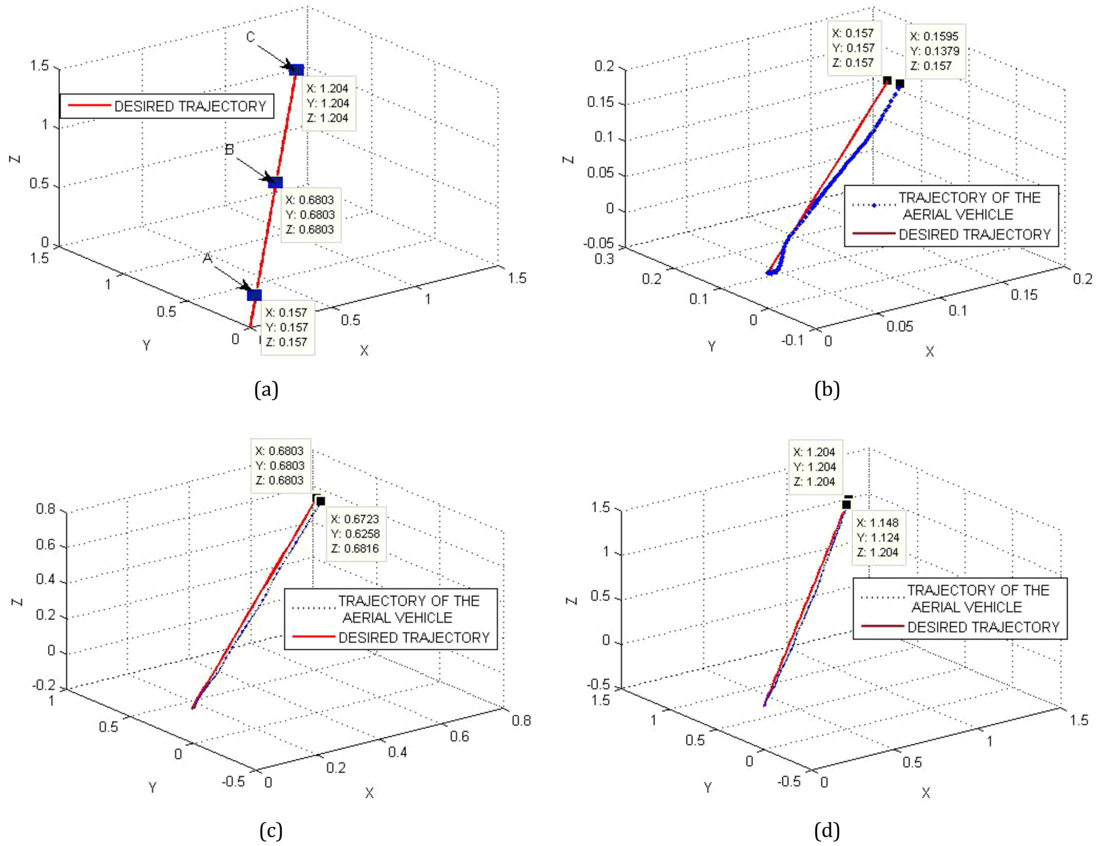

Fig. 15. (a) Indicates the desired trajectory for the aerial vehicle to travel with a constant increase in altitude. A, B and C are via points in the desired trajectory. (b)–(d) are 3D plots of the path traced by the aerial vehicle for 10, 40 and 70 path points indicated by A, B and C in (a), respectively.

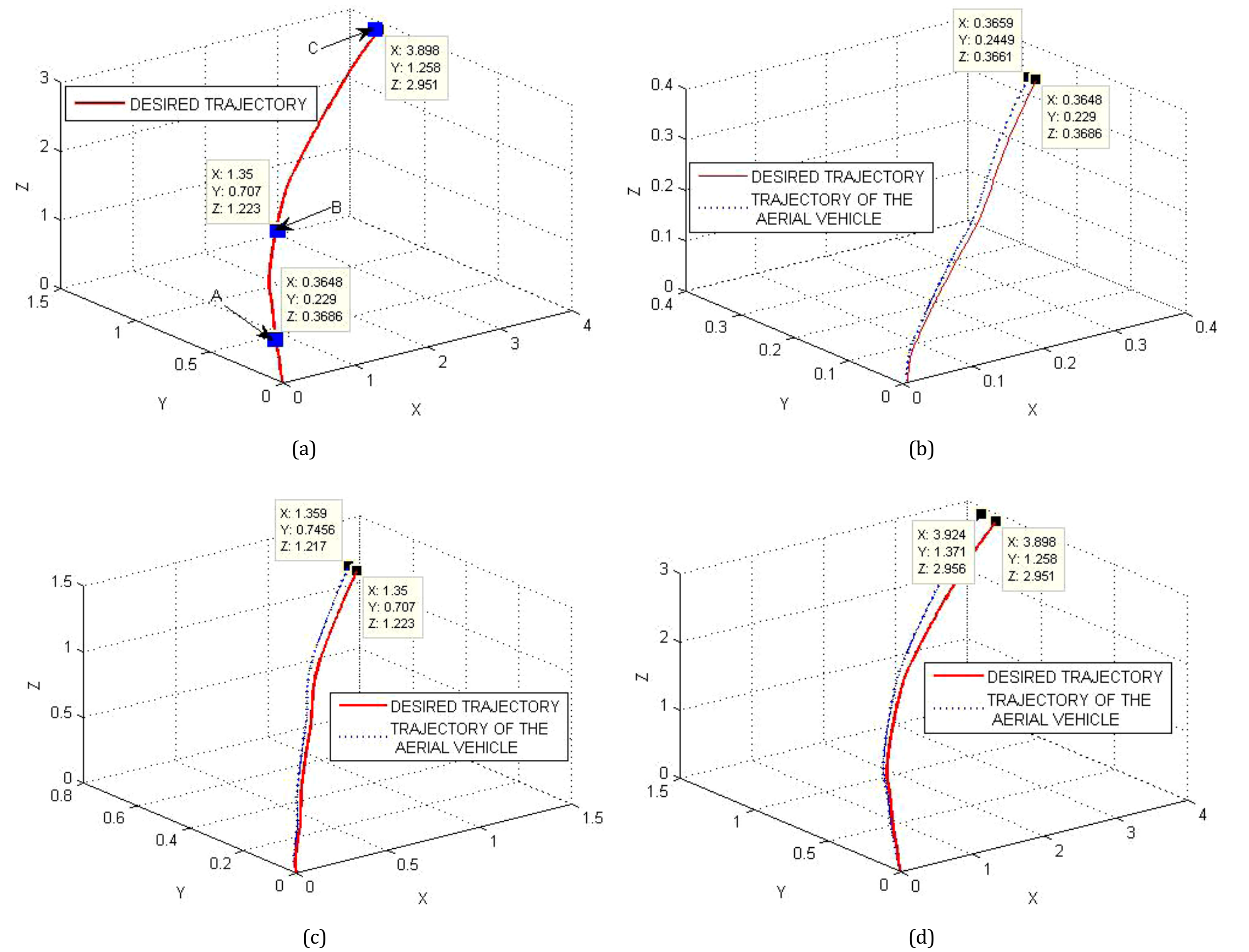

Fig. 16. (a) Indicates the desired trajectory for the aerial vehicle to turn right. A, B and C are via points in the desired trajectory. (b)–(d) are 3D plots of the path traced by the aerial vehicle for 20, 70 and 170 path points indicated by A, B and C in (a), respectively.

The aerial vehicle is to reach an altitude of 2–3 meters in all the simulations. It can be seen from Tables 4–6 that the errors in X, Y and Z positions at various path points are small and the TOF of the aerial vehicle at different path points are in the order of a few seconds. From Figs. 15–17, it is verified that for trajectories with less variations (example, to fly with a constant increase in altitude or when the magnitude of turn is less) the aerial vehicle is able to follow the trajectories closely after a few seconds of flight. But for trajectories requiring drastic changes in flight (example, to turn acutely left/right) the aerial vehicle deviates initially then follows the desired trajectory. In all the cases, the desired altitude is reached. Figure 18 shows the capacity of the aerial vehicle to turn left, turn right and fly in a stable manner with a constant increase in altitude. The aerial vehicle takes around 10–15 s to stabilize after taking off and then performs a stable flight. It is capable of turning left/right or left and right immediately without losing its stability and is able to regain the previous flight mode (i.e., constant increase in altitude).

5.3. *Evolutionary algorithm-based wingbeat parameter generation*

Evolutionary algorithms (EAs) are nature-inspired techniques for solving optimization problems. EAs are generally utilized when the search space for a problem is large and when there are many number of parameters that need to simultaneously optimized. EAs follow the biological model of evolution and natural selection for solving the problem. There are 18 wingbeat parameters that are to be generated for each degree of bird's wing beat. For a single wingbeat, $18 \times 360 = 6480$ parameters are to be calculated. This current problem can be considered as the optimization problem. The objective of the problem is to find wingbeat parameters for each wingbeat such that the error in desired

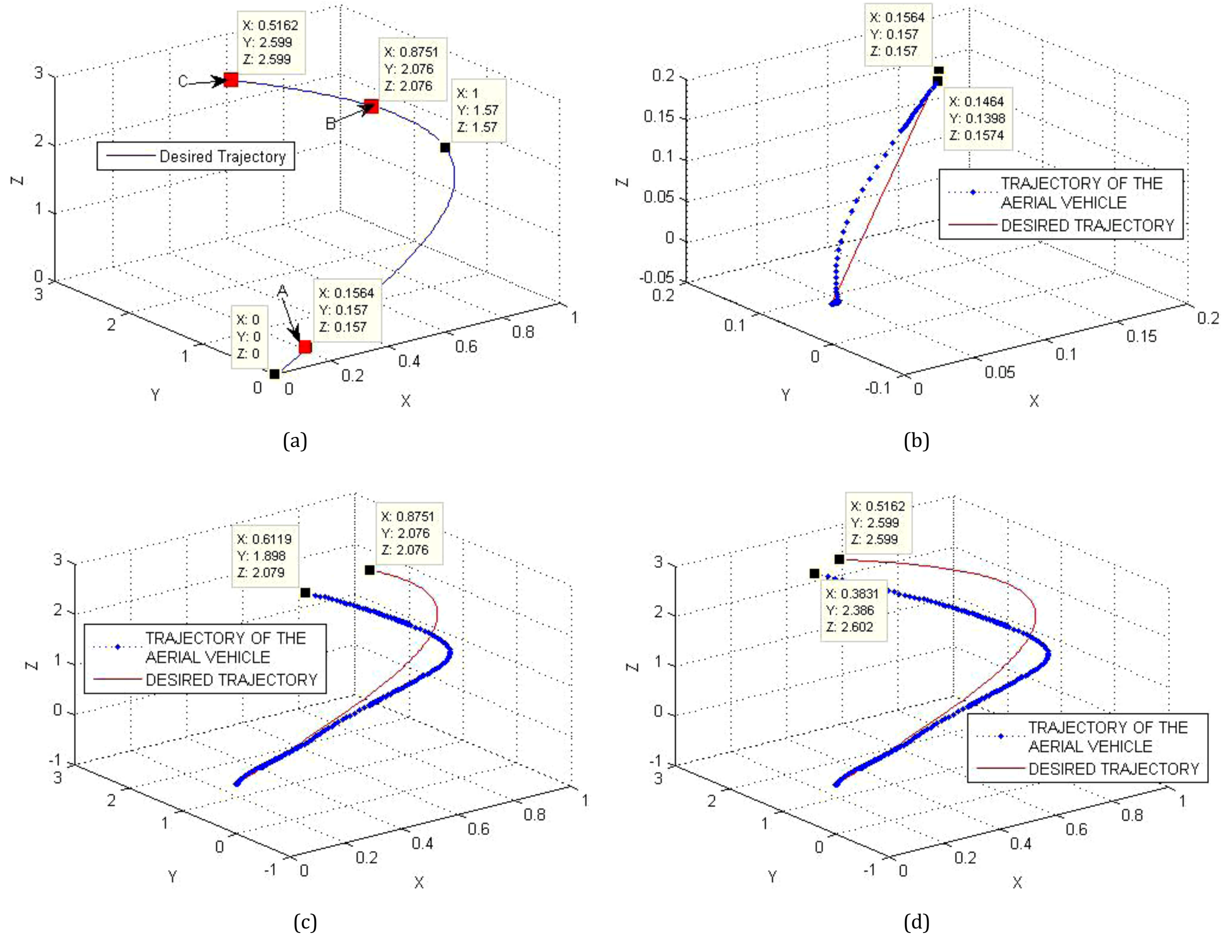

Fig. 17. (a) Indicates the desired trajectory for the aerial vehicle where A, B and C are via points in the trajectory. (b)–(d) are 3D plots of the path traced by the aerial vehicle for 10, 120 and 150 path points indicated by A, B and C in (a), respectively.

position to be reached and the position reached by the robot is minimized. Since a large number of parameters are to be identified to achieve an optimal solution, EAs are suitable for solving this problem. Genetic algorithm (GA), a type of EA, is utilized for obtaining wingbeat parameters for each wingbeat.

Table 4. Error at different path points and the time of flight (TOF) for each path point travelling on a straight trajectory.

Path points	Error-X (m)	Error-Y (m)	Error-Z (m)	TOF (s)
10	0.101	0.063	0.001	24
20	−0.0008	0.0294	−0.005	34
30	0.0042	0.0418	−0.0017	40
40	0.008	0.0545	−0.0013	45
50	0.0269	0.0646	−0.0017	52
60	0.0412	0.0746	−0.001	61
70	0.056	0.08	0	64

Table 5. Error at different path points and the time of flight (TOF) for each path point while turning right trajectory.

Path points	Error-X (m)	Error-Y (m)	Error-Z (m)	TOF (s)
3	−0.00027	−0.00409	−0.03131	13
20	−0.0025	−0.0159	0.0025	28
40	−0.002	−0.0216	−0.0053	40
60	−0.006	−0.0328	0.007	46
90	−0.016	−0.0523	0.006	54
120	−0.012	−0.07	0.009	63
140	−0.003	−0.087	0.012	66
170	−0.026	−0.113	−0.032	71

5.3.1. *Problem formulation*

There are 18 wingbeat parameters that need to be identified for each 1° of the wingbeat. Hence a vector with 18 elements is utilized as an individual. Each element of the

Table 6. Error at different path points and the time of flight (TOF) for each path point while turning left.

Path points	Error-X (m)	Error-Y (m)	Error-Z (m)	TOF (s)
10	0.01	0.0172	−0.0004	17
30	−0.0383	0.0511	−0.0023	28
50	−0.1444	0.0859	−0.0024	36
70	0.0296	0.1246	−0.0051	46
90	0.1901	0.1513	−0.0025	53
120	0.2632	0.1777	−0.0029	56
150	0.1331	0.2134	−0.0027	62

individual corresponds to a wingbeat parameter. These individuals are randomly initialized based on the maximum $\overline{u_i}$ and minimum $\underline{u_i}$ joint limits. Single point cross over is utilized as cross-over operator. The cross over and mutation operation are performed without violating the constrains of wingbeat parameters. The optimization problem is formulated as a minimization problem where the objective is to minimize the error between the desired position and the position reached by the robot. In-order to compare the performance of GA-based method and cosine wave-based method, the positions reached by the robot shown in Fig. 18 are utilized as desired positions. It is to be noted that the variables involved in estimating the position of the robot for each degree of movement of the wings (wingbeat angle Θ) are also dependent on their previous values. Algorithm 5.1 shows the algorithm for estimating wingbeat parameters using GA.

The GA successfully traced the trajectory obtained using cosine wave-based wingbeat generation. The difference in both the techniques lies in the computational cost. GA-based method requires 3.6×10^7 function evaluations for 1000 generations with a population size of 100. The cosine wave-based method requires only 360 function evaluations.

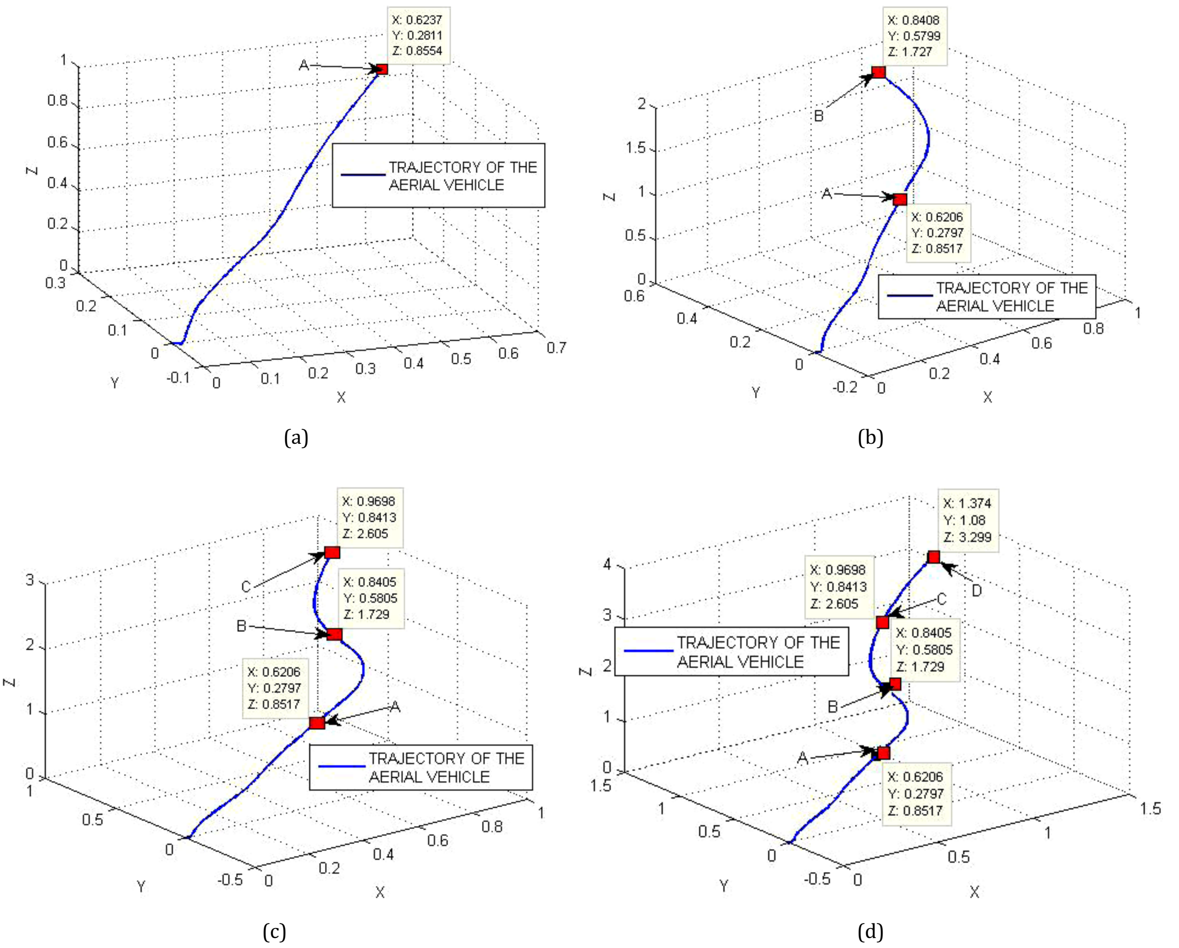

Fig. 18. (b)–(d) are 3D plots of the path traced by the aerial vehicle. (a) Indicates the trajectory of the aerial vehicle while it is stabilizing after take off. After stabilizing, the aerial vehicle increases its altitude in a linear manner. (b) Shows the aerial vehicle turning left and (c) Shows the aerial vehicle turning right immediately after turning left. (d) Shows the aerial vehicle moving with a linear increase in altitude in a stabilized manner.

Algorithm 5.1.

Require: Population pop, number of individuals in the population p_n, cross-over rate c_r, mutation rate m_r, maximum number of generations for evolution G, desired positions $D_p(d_x, d_y, d_z)$

```
Randomly initialize pop.
for i = 1 to p_n do
    Estimate P^i(p^i_x, p^i_y, p^i_z) based on the lift and drag
    forces generated for the current wingbeat parameters
    of the individual i.
    calculate mean squared error (MSE) between D_p and P^i
end for
for wingbeat angle Θ = 0° to 360° do
    while population number <= G do
        Rank the individuals based on the error of each individual.
        Do cross over where pop_cr is the new population after cross over.
        Do mutation where pop_m is the new population after mutation.
        Update population after cross over and mutation
        for i = 1 to p_n do
            Estimate P(p^i_x, p^i_y, p^i_z) based on the lift and drag
            forces generated for the current wingbeat parameters
            of the individual i.
            calculate MSE between D_p and P^i
        end for
    end while
end for
```

This shows that cosine wave-based method is 100,000 times computationally less expensive than the GA-based method. This demonstrates the real-time usability of the proposed cosine wave method.

6. Conclusion and Future Works

The main contribution of this paper is a general algorithm to generate the wingbeat parameters for a 15 DOF flexible-wing aerial vehicle and to ensure bird-like dynamic flight motions. The cosine wave-based functions employed produces results at a rate suitable for real-time implementation. The model of the aerial vehicle is based on a bird with appropriate physical, bio-mechanic and aerodynamic properties and it naturally performs a variety of aerial maneuvres. Proper parametrization of wingbeat parameters is essential to ensure flight motions similar to that of a real bird. At present, only continuous vortex gait is modeled into the system. In future, the vortex ring gait pattern can also be modeled. Other possibilities include changing the flapping frequency of the aerial vehicle dynamically depending upon the path to be followed and modeling the motions for landing sequences.

References

[1] G. S. P. Miller, The motion dynamics of snakes and worms, in *Proc. 15th Ann. Conf. Computer Graphics and Interactive Techniques* (1988), pp. 169–173.

[2] X. Tu and D. Terzopoulos, Artificial fishes: Physics, locomotion, perception, behavior, in *Proc. 21st Ann. Conf. Computer Graphics and Interactive Techniques* (1994), pp. 43–50.

[3] D. C. Kar, K. K. Issac and K. Jayarajan, Gaits and energetics in terrestrial legged locomotion, *J. Mech. Mach. Theory* **38** (2003) 355–366.

[4] W. Shyy, M. Berg and D. Ljungqvist, Flapping and flexible wings for biological and micro air vehicles, *Progress Aerosp. Sci.* **35** (1999) 455–505.

[5] S. A. Huber, M. O. Franz and H. H. Blthoff, On robots and flies: Modeling the visual orientation behavior of flies, *Robot. Auton. Syst.* **29**(4) (1999) 227–242.

[6] K. Senda, T. Obara, M. Kitamura, T. Nishikata, N. Hirai, M. Iima and N. Yokoyama, Modeling and emergence of flapping flight of butterfly based on experimental measurements, *Robot. Auton. Syst.* **60**(5) (2012) 670–678.

[7] W. Shyy, H. Aono, S. K. Chimakurthi, P. Trizila, K. C, C. E. S. Cesnik and H. Liu, Recent progress in flapping wing aerodynamics and aeroelasticity, *Progress in Aerosp. Sci.* **46** (2010) 284–327.

[8] Z. Kos, M. Nagy, S. Leven and T. Vicsek, Thermal soaring flight of birds and unmanned aerial vehicles, *Bioinspiration Biomimetics* **5**(4) (2010) 045003.

[9] K. Sims, Evolving virtual creatures, *21st Ann. Conf. Computer Graphics and Interactive Techniques* (1994), pp. 15–22.

[10] J. V. Leeuwen and J. L. Van, Modelling muscular hydrostats: Relationships between form and function source, *Math. Comput. Model. Biol. Syst.* (2002) 127–151.

[11] A. A. Biewener, *Animal Locomotion* (Oxford University Press, 2003).

[12] M. B. Abbot and D. R. Basco, *Computational Fluid Dynamics: An Introduction for Engineers* (Longman Science and Technology, London, 1989).

[13] J. M. V. Rayner and R. Gordon, Visualization and modelling of the wakes of flying birds. In *Biona Report, No. 13, Motion Systems*, R. Blickhan, A. Wisser and W. Nachtigall (eds.), (Jena, Gustav Fischer Verlag, 1998), pp. 165–173.

[14] C. Henderson and S. Adams, *Birds in Flight: The Art and Science of How Birds Fly* (MBI Publishing Company, 2008).

[15] T. J. Mueller, Aerodynamic measurements at low Raynolds numbers for fixed wing micro-air vehicles, Tech. Rep., DTIC Document (2000).

[16] H. Liu, X. Wang, T. Nakata and K. Yoshida, Aerodynamics and flight stability of bio-inspired, flapping-wing micro air vehicles, in *Autonomous Control Systems and Vehicles, Intelligent Systems, Control and Automation: Science and Engineering*, K. Nonami, M. Kartidjo, K.-J. Yoon and A. Budiyono (eds.), Vol. 65 (Springer, Japan, 2013), pp. 145–157.

[17] K. Takizawa, N. Kostov, A. Puntel, B. Henicke and T. Tezduyar, Space-time computational analysis of bio-inspired flapping-wing aerodynamics of a micro aerial vehicle, *Comput. Mech.* **50**(6) (2012) 761–778.

[18] D. Doman and M. Oppenheimer, Method for shaping wing velocity profiles for control of flapping wing micro air vehicles (April 2014), US Patent 8,700,233.

[19] C. W. Reynolds, Flocks, herds and schools: A distributed behavioral model, *Comput. Graph.* **21**(4) (1987) 25–34.

[20] B. Ramakrishnananda and K. C. Wong, Animating bird flight using aerodynamics, *Vis. Comput.* **15**(10) (1999) 494–508.

[21] J. Wu and Z. Popovic, Realistic modelling of bird flight animations, *ACM Trans. Graphics* (2003) 888–895.

[22] C. Zhu, K. Muraoka, T. Kawabata, C. Cao, T. Fujimoto and N. Chiba, Real-time animation of bird flight based on aerodynamics, *J. Arts Sci.* **5**(1) (2006) 1–10.

[23] B. Parslew and W. J. Crowther, Simulating avian wing-beat kinematics, *J. Biomech.* **43** (2010) 3191–3198.
[24] D. B. Baier, S. M. Gatesy and F. A. Jenkins, A critical ligamentous mechanism in the evolution of avian flight, *Nature* **445** (2007) 307–310.
[25] U. M. Norberg, *Vertebrate Flight* (Springer-Verlag, 1990).
[26] C. J. Pennycuick, Predicting wingbeat frequency and wavelength of birds, *J. Exp. Biol.* **150** (1990) 171–185.
[27] S. Heathcore, Z. Wang and I. Gursul, Effect of spanwise flexibility of flapping wing propulsion, *J. Fluids Struct.* **24** (2008) 183–199.
[28] M. W. Oppenheimer, D. O. Sigthorsson and D. B. Doman, Controllability analysis for a flapping-wing mav with power and control actuators, *Am. Control Conf.* (2010), pp. 33–38.
[29] T. J. Muller, *Fixed and Flapping Wing Aerodynamics for Micro Air Vehicle Applications* (AIAA, Reston, USA, 2001).
[30] A. Colozza, Fly like a bird, *IEEE Spectrum* **44** (2007) 38–43.
[31] B. Parslew, Low order modelling of flapping wing aerodynamics for real-time model based animation of flapping flight, Master's thesis, University of Manchester (2005).

Willson Amalraj Arokiasami, received his B.E. (Electronics and Instrumentation Engineering) from Anna University Chennai, India in 2010, and his Masters in Electrical Engineering (2012) and Ph.D. in Electrical and Computer Engineering (2016) from National University of Singapore (NUS). His research interests include motion planning, perception and localization of unmanned mobile robots, computer vision, multi-agent systems and autonomous control of unmanned aerial and ground vehicles. Willson is currently an Instructor at the Engineering Design and Innovation Centre (EDIC) at NUS, where he focusses on providing innovative design solutions for autonomous systems.

Prahlad Vadakkepat an Associate Professor at the National University of Singapore is the founder secretary of the Federation of International Robot-soccer Association and its General Secretary during 2000–2016. He is one of the resource persons in the Igniting Minds movement by Vijyana Bharathi India which is a programme enabling students to shed conventions and think out of the box. Vadakkepat is the Editor-In-Chief for the Springer Reference book on Humanoid Robotics. He is an associate editor of the International Journal of Humanoid Robotics. His Humanoid robots and robot soccer teams have consistently won several international prizes.

Vadakkepat received his M.Tech and Ph.D. from Indian Institute of Technology Madras, in 1989 and 1996 respectively. Since 1999, he is with the National Univ. of Singapore. His research interest include Frugal Innovation, Distributed robotic systems, Humanoid robotics, Biomorphs, Neuro-Fuzzy Controllers and Intelligent Control techniques.

Abdullah Al Mamun, as Associate Professor at the National University of Singapore, received his B.Tech (Hons) and Ph.D. in 1985 and 1997, respectively. Before joining the faculty of NUS, he has worked for industry and research institutes including Siemens, Maxtor and Data Storage Institute (Singapore). His research interests include mechatronics, precision control systems and control of mobile robots.